Interconnected activated carbon nanofiber derived from mission grass for electrode materials of supercapacitor

Rika Taslim[1], **Muhammad Ihsan Hamdy**[1], **Merry Siska**[1], **Erman Taer**[2], **Deris Afdal Yusra**[2], **Apriwandi**[2], **Marhama Jelita**[3], **Susi Afriani**[3] **and Novi Gusnita**[3]

[1] Department of Industrial Engineering, State Islamic University of Sultan Syarif Kasim, 28293 Simpang Baru, Riau, Indonesia
[2] Department of Physics, Faculty of Mathematics and Natural Sciences, University of Riau, 28293 Simpang Baru, Riau, Indonesia
[3] Department of Electrical Engineering, State Islamic University of Sultan Syarif Kasim, 28293 Simpang Baru, Riau, Indonesia

E-mail: rikataslim@gmail.com

CrossMark

Abstract

The porous carbon electrode materials for supercapacitors derived from biomass waste attract lots of attention due to their natural abundance and low cost. This study therefore aims at developing a cost-effective and sustainable method for synthesising porous activated carbon derived from mission grass biomass waste (MG). The one-stage integrated pyrolysis for carbonisation, physical activation, and KOH activation was used to obtain porous activated carbon monolith. The surface morphology and pore structures consist of interconnected activated carbon nanofiber with high carbon content of 90.45%. The KOH impregnation successfully changed the morphology from the rod-like shape into a nanofiber structure. Due to their synergistic effect, the specific capacitance enhanced from 115 to 171 F g^{-1} in 1 M H_2SO_4 aqueous electrolyte with an egg duck shell membrane as a separator. The result showed that the maximum energy and power densities were 23.75 Wh kg^{-1} and 96.94 W kg^{-1}, respectively. Therefore, these unique properties enable the mission grass to become a high potential for porous carbon electrode materials as supercapacitor energy storage.

Keywords: nanofiber, porous carbon, electrode materials, supercapacitor, energy storage

1. Introduction

Energy is a basic necessity for humans all over the world, as well as water and food. Its consumption tends to increase significantly every year, thereby lowering the availability of fossil fuels as the main energy source. This led to the development of numerous renewable energy technologies such as solar cells, turbines, and wind power, as an alternative electricity generation. The availability of these resources is still limited, therefore, storage devices with high energy and power densities, as well as excellent rate performance such as batteries, supercapacitors, and electrolyte capacitor are needed [1, 2]. Furthermore, supercapacitor is a type of energy storage device that is considered to have high performance due to their relatively higher energy density than capacitors and greater power density than batteries [3, 4]. The electrode material is the main substance used in the production of high-performance supercapacitors, including electric double-layer capacitors (EDLC) and pseudo-capacitor [3, 5]. Due to the high surface area, better electrical conductivity, and more stable electrochemical properties of porous carbon, it is defined as the ideal electrode material for EDLC [6]. The porous carbon materials often used are nanotubes, activated carbon, graphene [7], and metal-organic [5, 8]. Conversely, the electrodes for pseudo-capacitive material used to store high energy from redox reactions are derived from metal

oxide transitions [9] and conductive polymers [10]. All electrode materials from both types of supercapacitors have superior properties such as numerous pore structures, highly accessible surface areas, and unique nanostructure morphology. These features contribute to provide abundant pathways for ion diffusion, more massive active sites for electrochemical reactions, and enhanced energy output [3, 11–13]. However, there are challenges associated with the preparation of supercapacitor electrodes such as its expensive cost, complex synthetic materials, multi-step preparation methods, and relatively complicated.

Presently, many studies reported the potential of biomass as an active carbon base material for supercapacitor electrodes with relatively low-cost preparation and environmental advantages [14–16]. In addition, the basic components of biomass such as C, H, O and N elements provide a significant advantage in the pseudo-capacitive behaviour. In addition, biomass raw material has a unique morphological structure of complex lignocellulose compounds such as nanomaterial including nanofiber, nanosheet, and nanospheres, as well as the interconnection between micro, meso and macroporous [17–19]. The synergy of these benefits increases energy in EDLC. For example, nanofiber and nanosheet structures were obtained from leaves-based with specific capacitance range of 25–150 F g^{-1} [20, 21]. In addition, Wang *et al* converted pinewood to activated carbon nanofiber via solar pyrolysis which produces an excellent specific capacitance of 349 F g^{-1} [22]. However, all of biomass wastes do not always exhibit nanostructures of porous carbon materials for supercapacitor. Therefore, it is necessary to know the potential biomasses that contain an effective lignocellulose content to produce nanostructure materials.

Mission grass (*Pennisetum polystachyon*) is one of the weeds commonly found in Indonesia, Philippines, Thailand, and Malaysia. This plant belongs to the Poaceae family and grows wildly. In Indonesia, mission grass is widely cultivated for livestock feed purposes, and it is rich in lignocellulose complex compounds and consists of 39.8%–40.0% cellulose, 23.3%–29.2% hemicellulose, 6.2%–14.6% lignin, and 3.3%–7.5% ash [23]. Therefore, it is potentially converted as activated carbon to supercapacitor electrodes.

This study aims to convert mission grass waste into interconnected macroporous and mesoporous carbon using effective-cost, simple methods for supercapacitor electrodes as high-performance energy storage devices. One of the stage integrated pyrolysis used for both carbonization and physical activation is KOH impregnation, which is selected to convert lignocellulose mission grass into activated carbon. Electrodes were then fabricated in the coin type with 1 M H$_2$SO$_4$ as aqueous electrolyte. The results showed that the activated carbon exhibits interconnected macropore and mesopore structures. Furthermore, the KOH impregnation successfully changes the morphology structure from the rod-like shape into the nanofiber. The symmetric capacitor double layers show maximum specific capacitance of 171 F g^{-1} at a scan rate of 1 mV s^{-1} in a two-electrode system. These unique properties enable the mission grass to become a high potential

for porous carbon electrode materials as supercapacitor energy storage.

2. Experimental section

2.1. Preparation of porous carbon monolith

The mission grass (MG) waste is collected from swampy areas located in Pekanbaru, Riau Province. This biomass waste is cut and cleaned with distilled water and dried in an oven at 110 °C. Approximately 30 g of the sample is pre-carbonised in an oven at 250 °C and converted into powder using ball milling. Furthermore, the pre-carbonised powder samples were impregnated with KOH solution using three different concentrations of 0.3, 0.5, and 0.7 M in a hot plate at a temperature of 80 °C and 300 rpm. These different concentrations produced samples of MG0.3, MG0.5, and MG0.7, respectively, which are dried after 2 days. Carbon powder is converted into the monolith form using a hydraulic press with the one-stage pyrolysis at room temperature to a maximum temperature of 600 °C in an N$_2$ gas environment, followed by the physical activation at high temperature of 850 °C at a CO$_2$ gas atmosphere. Finally, the carbon monolith samples were neutralized using distilled water.

2.2. Materials characterisation

The density analysis was evaluated in accordance with the dimension, mass, and volume of porous carbon monolith. Thermal analysis was carried out using thermogravimetric analysis (TG/DTG) and Shimadzu TGA-50 at heating and flow rates of 10 °C min^{-1} and 100 ml min^{-1}, respectively in N$_2$ atmosphere. The degree of crystallinity of the carbon monolith was characterized by powder X-ray diffraction (XRD) method using the Phillip X-Pert Pro PW3060/10 instrument at a Cu-K_α radiation. In addition, the surface morphology and chemical composition of the samples were investigated to determine their scanning electron microscopy and energy dispersive spectroscopy (EDS) using the JEOL-JSM-6510LA instrument with an applied voltage of 15 kV. The porosity properties of the samples were reviewed using N$_2$ gas adsorption/desorption analysis with a Quantachrome TouchWin Version 1.2 instrument at degassing temperature of 300 °C.

2.3. Electrochemical measurement

The electrochemical performances of porous carbon monolith as supercapacitor electrodes were evaluated in the cyclic voltammetry (CV) by using a CV UR Rad-Er 5841 instrument calibrated by VersaStat II Princeton Applied Research, at an error rate of ±6.05%. Furthermore, the evaluated supercapacitor cell consists of a porous carbon monolith in the two-electrode system of 1M H$_2$SO$_4$ as an electrolyte assembled in coin type. The membrane egg duck shell was selected as a separator with the specific capacitance evaluated by using the standard equation. The potential window was
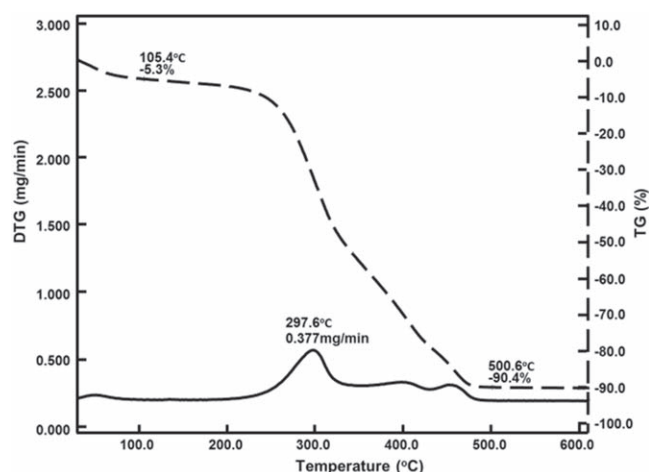
Figure 1. TG/DTG curve for pre-carbonised mission grass powder.

applied in a range of 0–1 V in different scanning rates of 1, 2, 5, and 10 mV s^{-1}.

3. Result and discussion

3.1. Thermal analysis

The carbonization process is an important factor used to convert biomass into porous carbon materials. Its temperature has a large influence on the pyrolysis process, and it is an essential factor in determining the carbon content of decomposed lignocellulose. The temperature suitable for the carbonization of porous carbon in the N$_2$ atmosphere was investigated using the TG/DTG analysis, as shown in figure 1. The differential thermal analysis/DTG shows two stages of significant weight loss with an increase in temperature. In the first stage, a weight-loss of 5.3% at a temperature of 105.4 °C was obtained with a drying and preheating stage caused by moisture evaporation [24, 25]. The second stage of weight-loss is found in the temperature range of 250 °C–500 °C at 85.1%. This stage correlates with the decomposition of lignocellulose compounds, including hemicellulose, cellulose, and lignin at different temperature ranges of 150 °C–215 °C [26]. Furthermore, the temperature of thermal degradation for cellulose is higher in the range of 300 °C–400 °C due to its regular structure and good thermal stability. In addition, cellulose has a relatively homogeneous unit, therefore, the pyrolysis temperature range is relatively narrow, at approximately 100 °C, capable of producing more volatile matters within a short time and less amount of solid residues [27, 28]. However, the lignin compound was decomposed in the high-temperature range of 190 °C–900 °C, and at 600 °C no further significant decrease was observed, with a total weight loss of 90.4% [28]. This phenomenon shows that the optimal carbonisation temperature of the activated carbon preparation is 600 °C.

Furthermore, the thermal gravimetry (TG) profile shows the rate of weight loss of the sample with increasing temperature. The instrument does not indicate a significant peak from room temperature to 250 °C. The rate of weight loss
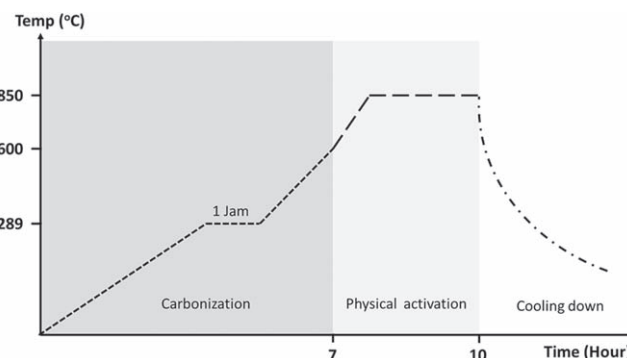

Figure 2. Profile of the one-stage integrated pyrolysis process.

dramatically increases from 250 to 297.6 °C at 0.377 mg min^{-1}. This phenomenon is indicated by the degradation of lignocellulose compounds, which occurs simultaneously [27, 28]. Hemicellulose, cellulose, and lignin are maximally decomposed, thereby creating the most significant weight loss. In the second stage, this analysis is related to DTG. Further temperature increases are no longer observed due to the rise in mass loss. Therefore, an initial temperature of 297.6 °C was used for 1 h during the carbonization process. The selection of initial and maximum carbonization temperature is expected to decompose lignocellulose compounds and modify the structure of porous carbon, which is advantageous for the performance of supercapacitor electrodes. Figure 2 shows a detailed analysis of the carbonization and physical activation of the pyrolysis process.

3.2. Density and degree of crystallinity behaviour

The one-stage integrated pyrolysis process for the carbonization and physical activation of carbon has a profound effect on physicochemical properties, which includes porous monolith. Density is the initial analysis of physical properties obtained at the end of the pyrolysis and chemical activation processes. The carbonization and physical activation of the pyrolysis process gradually reduces the density of monolith carbon, as shown in figure 3(a). The carbonization from room temperature to a maximum temperature of 600 °C reduces and decomposes all complex compounds, including moisture, hemicellulose, cellulose, and lignin in the TG/DTG analysis. This process allows an increased carbon content and provides porosity effect on carbon monoliths, thereby reducing mass and volume. However, the co-product of carbonization in the form of solid tar covers the formed pores. Therefore, it is necessary to activate it with high temperature [29]. Physical activation from a temperature of 600 °C–850 °C eliminates co-product carbonization that covers the pore and exhibits a relatively better pore structure [19, 29].

In addition, it is also possible to produce interconnected pores such as meso and macropores. This phenomenon reduces the density of porous carbon monoliths and enhances the performances of supercapacitor electrodes. Figure 3(a) shows that all samples have decreased density at the end of the one-stage pyrolysis process. Furthermore, three different KOH activators, namely 0.3, 0.5, and 0.7 M applied in all
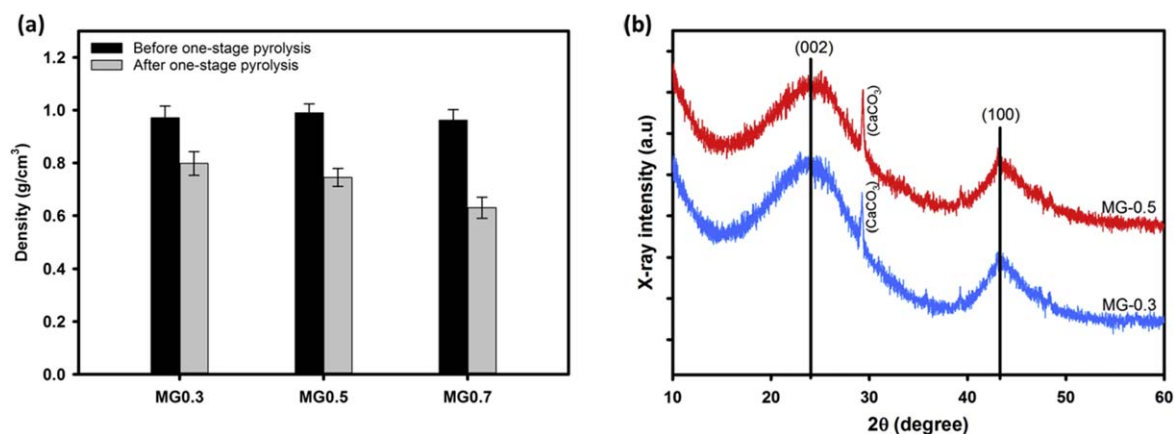
Figure 3. (a) Density of porous carbon, (b) XRD pattern of porous carbon.

samples, showed a significant effect on density. The addition of KOH concentrations from 0.3 to 0.7 M has the ability to reduce the density from 25 to 46%, thereby creating more connected pores in the porous carbon monoliths [30]. This analysis correlates with the use of SEM and N_2 gas adsorption described in the following subsection.

The crystal structures of porous carbon monolith were analysed using the XRD pattern. This created a significant broad peaks at $2\theta = 23.2°–25.3°$ and $44.5°–45.7°$ which corresponded to (002) and (100) reflections in both MG0.3 and MG0.5 samples with a typical carbon characteristic of JCPDS No. 41–1487. This result is similar to other reports such as porous carbon derived from baobab fruit shell [31], banana stem [30], and argan [32] which showed the appearance of broadening peaks at 23 and 43°, 24 and 44°, and 25 and 43°, respectively. All broad peaks showed a typical amorphous carbon structure. However, the broadness of XRD peaks was found to largely shift at (002) diffraction from 23.2 to 25.3 in the MG0.5 when compared with MG0.3. The carbon structure is more amorphous by KOH activation at a higher concentration from 0.3 to 0.5 M, and this result correlated with SEM analysis to produce more interconnected meso- and macropores in MG0.5 porous carbon monolith. Furthermore, the XRD pattern also observed a sharp peak at 2θ of 29.6°, which indicated the presence of calcium carbonate ($CaCO_3$) (JCPDS No. 82–1690) in both MG0.3 and MG0.5. Meanwhile, more addition of KOH concentrations from 0.3 to 0.5 M reduces the $CaCO_3$ compound in porous carbon monolith, with a higher concentration in MG0.5 XRD pattern. This existence is extracted from the common content of calcium in biomass materials, which is confirmed by EDS analysis.

3.3. Surface morphology and porous properties

The surface morphology and pore structure of porous carbon monolith derived from mission grass biomass waste material are characterised by scanning electron microscopy, as shown in figure 4. The pyrolysis process and impregnation of the chemical reagent are used to change and control the surface morphology. Furthermore, the one-stage integrated pyrolysis, as well as the carbonisation and physical activation processes,

is used as the binding chains of the lignocellulose components to separate hemicellulose and lignin from the cellulose contents. The original shape of cellulose is rod-like, and at high temperatures, it has the potential to be microfiber and nanofiber [33], while hemicellulose and lignin tend to form globular morphology [16, 33, 34]. At high temperature, the activation process has the potential to form nanosheet and nanosphere structures, as previously reported [35, 36]. Furthermore, KOH activation is beneficial for larger SSA with suitable porous and interconnected pore structure. These benefits are contributing factors as the ion pathways for higher powers and specific capacitance supercapacitor electrode [37, 38].

The SEM micrograph of MG0.3 and MG0.5 samples showed that similar morphology consists of the carbonaceous fragments with irregular sizes, ranging from several hundreds of micrometers, as shown in figures 4(a) and (b). Furthermore, MG0.3 sample exhibited a structure of the aggregated porous-flakes with apparent macropores. The thermochemical decomposition of KOH causes the etching of solid carbon chains in the sample and produces morphology flaky-like shapes with macropores in a range of 234 nm, as shown in figure 4(b). In addition, the morphology of a short rod-like shape has a diameter of 23 nm.

Figure 4(c) showed rougher and hollow-fiber samples of MG0.3 and MG0.5 with clear macropore and mesopore structures. In particular, there are many sub-macropores in this amorphous structure, therefore, the addition of KOH concentration has the ability to modify the structure and morphology of porous carbon monoliths. The MG0.5 pyrolysed at high temperatures obtained hierarchical interconnected porous structures, as shown in figure 4(d), however, undeveloped micropores, as seen in the pore distribution curves. An increase in KOH concentration to 0.5 M creates more carbon chains and widens the pores due to high-temperature pyrolysis, and obtains interconnected pores hierarchically. In addition, microfiber structures are also found on GM0.5 samples due to the addition of KOH activator, which decomposes the hemicellulose and lignin attached to cellulose and further reduces the size of rod-like cellulose to microfiber. This interconnected mesopores and
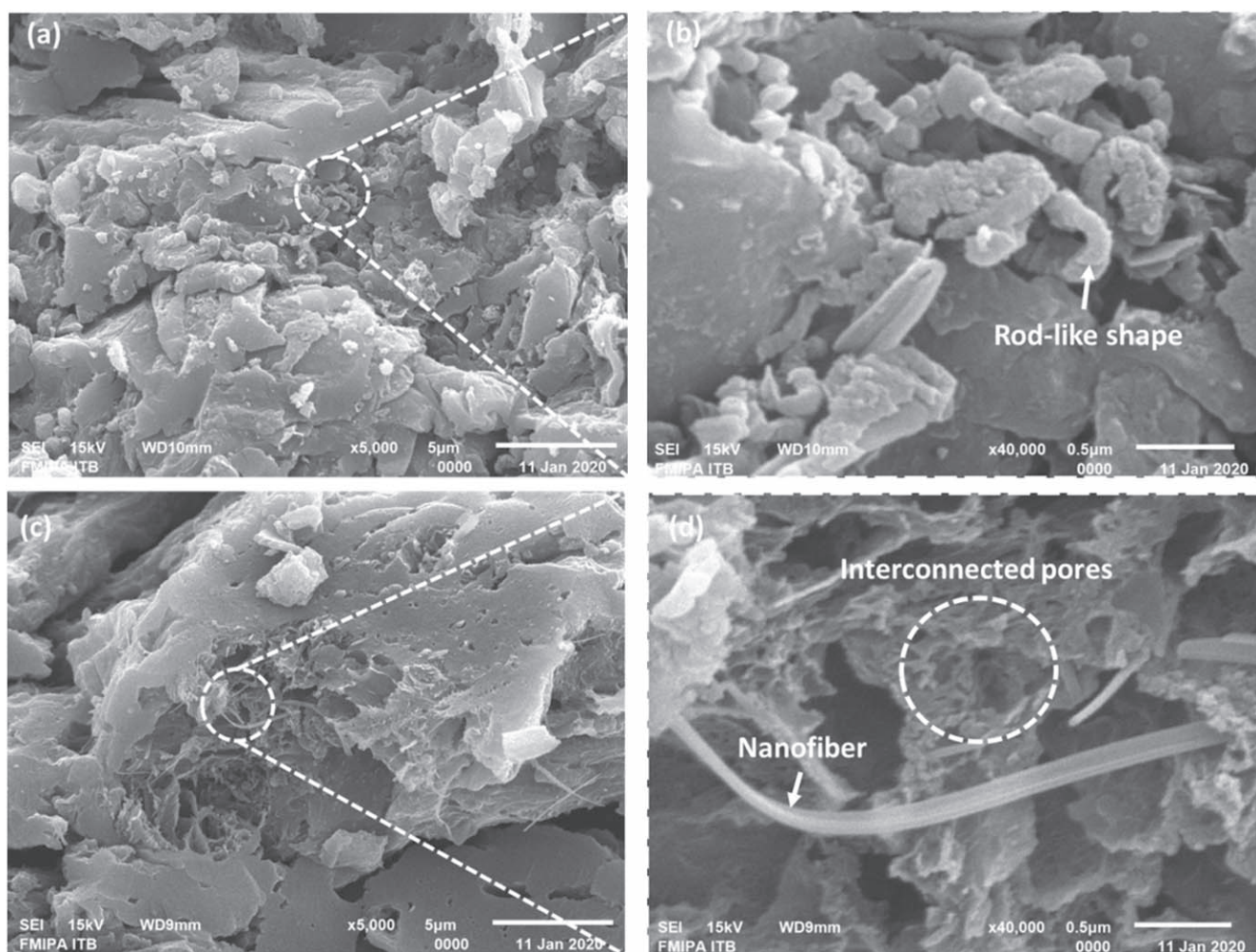
Figure 4. SEM images for (a) MG0.3, (b) enlarge of MG0.3, (c) MG0.5, (d) enlarge of MG0.5.

macropores with decorated microfiber structures make a high contribution to the surface area, and ion transfer on the electrode/electrolyte interface, thereby increasing the supercapacitor performance, as confirmed by the analysis of N_2 gas absorption and the cyclic voltammetry curve. In general, there is a unique interconnection between mesopore and macropore structures, which interacts with MG biomass, one-stage pyrolysis, and KOH activation, thereby, producing a carbon framework and small gas molecules of H_2O, CO_2, and CO [27], to form micropores. However, when carbon is pyrolysed at high temperatures in one stage, its micropores are integrated with larger sizes destroyed to form stable structures of distributed mesopores and macropores. This unique structure is far more useful for the transportation and storage of electrolyte ions, thereby increasing the performance of supercapacitor electrodes.

Figure 5(a) shows the N_2 gas adsorption/desorption curves for MG0.3 and MG-0.5 samples used to observe the porous behaviour of carbon monolith. Generally, both MG-0.3 and MG-0.5 profiles exhibit a combination of types I and IV based on IUPAC classification [39]. The significant increase of N_2 gas adsorption at a relative low pressure of $P/P_0 < 0.1$ suggests a small amount of microporous structure

[40]. The hysteresis loop with a typical H4 type at a relative pressure of $P/P_0 = 0.4–0.95$ indicates the presence of numerous mesopores [41]. However, all samples do not show an ideal H4 type of hysteresis because at a relative pressure $P/P_0 < 0.4$, the desorption line fails to blend with the adsorption, which indicates that the presence of N_2 gas is trapped in the carbon monolith pores [42]. This phenomenon is caused by the formation of like-bottle pores, which have a narrow pore neck enabling it to hold the N_2 gas till the desorption process is complete [43]. Furthermore, the MG-0.5 sample showed a significant increase in the relatively high pressure of $P/P_0 = 0.9–0.98$, indicating that there are a lot of macropores not found in the MG-03 sample. The specific surface area for both samples was evaluated using the BET method of 152.072 and 266.159 m g^{-1} for MG-0.3 and MG-0.5 samples, respectively. The addition of KOH concentrations from 0.3 to 0.5 M increased the specific surface area and affected the number of carbon monolith pore combinations confirmed by the N_2 gas absorption profile. In the MG-0.5 sample, real interconnected pores are formed, which comprise micropores, mesopores, and macropores, which are not found in MG0.3. These pore combinations greatly contribute to
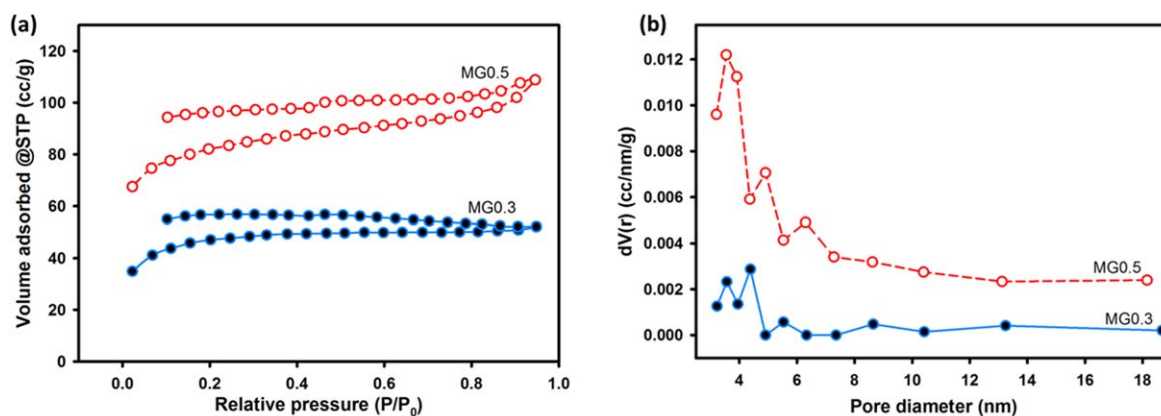
Figure 5. (a) N_2 gas adsorption curve of MG0.3 and MG0.5, (b) Pore size distribution of MG0.3 and MG0.5.

Table 1. The chemical composition of both MG-0.3 and MG-0.5 samples.

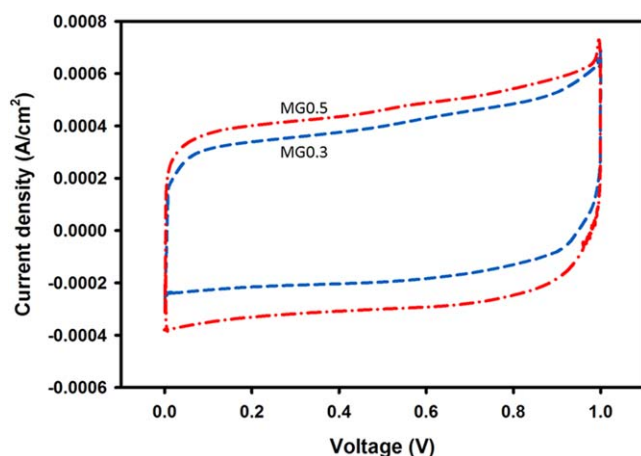| Element contents	C (%)	O (%)	Na (%)	Si (%)	K (%)	Ca (%)
MG0.3	88.41	9.47	0.54	0.85	0.46	0.28
MG0.5	90.45	7.67	0.55	0.23	0.90	0.20

Figure 6. CV curve for MG-0.3, MG-0.5, and MG-0.7 samples.

Table 2. The specific capacitance, energy, and power densities of MG0.3 and MG0.5 supercapacitor cells.

Supercapacitor cells	C_{sp} (F g^{-1})	E (Wh kg^{-1})	P (W kg^{-1})
MG0.3	115	15.97	57.55
MG0.5	171	23.75	85.58

providing electrolyte ion active sites, thereby increasing the ion diffusion rate into the electrode interface [44].

These results confirmed the presence of XRD and SEM analyses. In addition, the pore distribution was evaluated using the BJH method for MG0.3 and MG0.5 samples. Figure 5(b) shows the pore diameter distribution profiles, both samples confirm mesopore size in the range of 3 to 20 nm. Furthermore, the addition of KOH concentration increases the average pore diameter from 3.2 to 3.5 nm for MG0.3 and MG0.5 samples. Conversely, the presence of mesopores in

MG0.5 samples is greater than in MG0.3, which has the ability to increase the surface area and interconnection in all pores.

3.4. Energy dispersive spectroscopy analysis

Furthermore, the chemical composition of MG0.3 and MG0.5 was reviewed by using energy dispersive spectroscopy (EDS), which was summarised in table 1. The porous carbon monolith preparation derived from mission grass waste successfully exhibited high carbon content at a percentage of 88.41%–90.45%. The increasing KOH concentration showed no significant effect on the percentage of carbon content.

Oxygen is the highest element after carbon, with a percentage of 7.67%–9.47%, which influences the hydrophilic behaviour [45]. The other elements are also found in a relatively low percentage such as sodium, silica, potassium, and calcium, which are related to compounds commonly found in biomass as raw materials [46]. The results obtained at EDS correlate with several previous reports that use biomass as a raw material of carbon monoliths such as bamboo [47], pineapple leaves [48], rice husk [49], and banana stem [30].

3.5. Electrochemical properties

The electrochemical behaviours and capacitive performances of the carbon electrodes derived from mission grass waste were evaluated in the two systems using 1 M H_2SO_4 electrolyte with potential windows of 0–1 V. Figure 6 shows the cyclic voltammetry (CV) profiles of MG0.3 and MG0.5 at a scan rate of 1 mV s^{-1}. All the profiles exhibit quasi-rectangular shapes, thereby leading to an ideal symmetric capacitor double-layer behaviour [50]. Furthermore, the area of quasi-rectangular shape indicates the specific capacitance of the
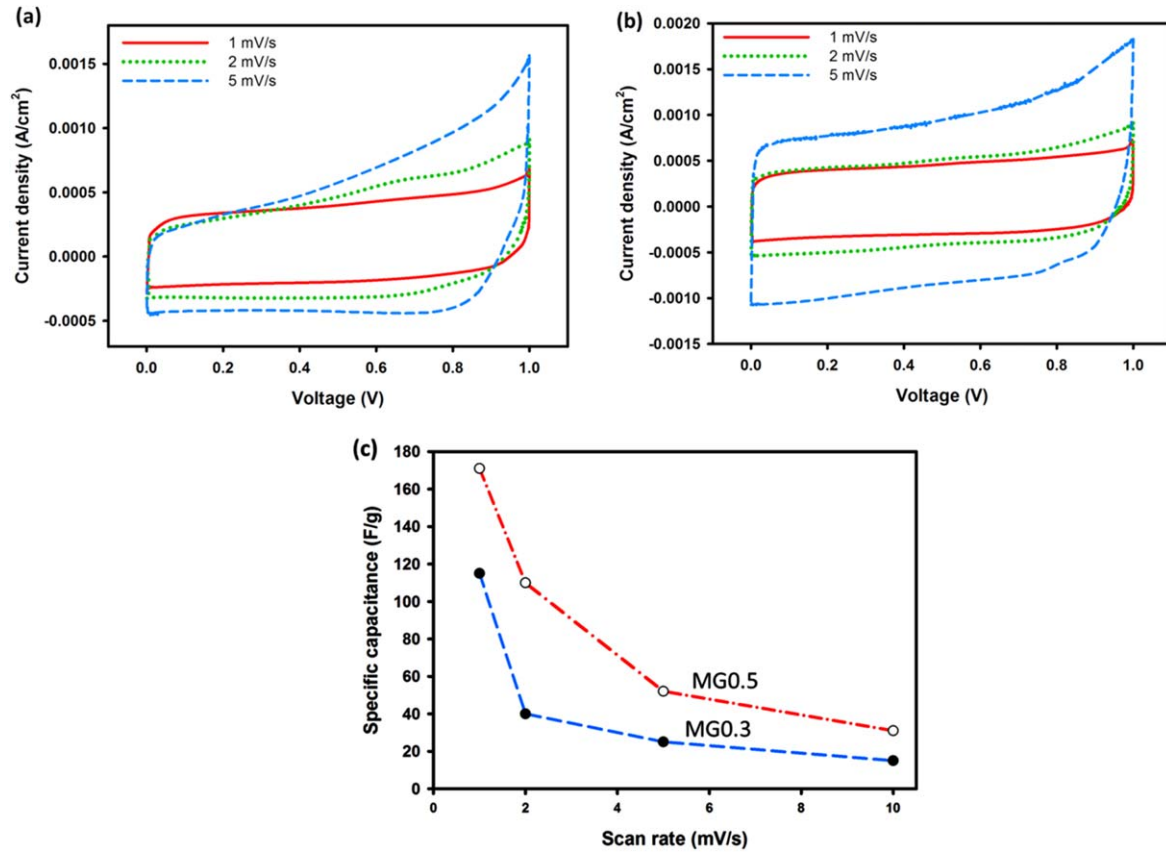
Figure 7. CV curve at various scan rates of (a) MG0.3, (b) MG0.5, and (c) specific capacitance versus scan rate variations for all samples.

Table 3. The comparing the electrochemical behaviour with other carbon-based.

Sources	Morphological structure	C_{sp} (F g^{-1})	Electrolyte	References
Banana steam	Nanofiber	74	1 M Na$_2$SO$_4$	[53]
Waste shaddock	Hierarchical porous	148	1 M H$_2$SO$_4$	[54]
Cattail fiber	Nanofiber	38.59	1 M H$_2$SO$_4$	[55]
Mangosteen peel	Stone	114.8	6 M KOH	[56]
American poplar fruit	Tubular-like	58.71	6 M KOH	[57]
Chitin seafood	Nanofiber	95	6 M KOH	[58]
Pineapple crown	Nanofiber	150	1 M H$_2$SO$_4$	[48]
Mission grass	Nanofiber	171	1 M H$_2$SO$_4$	This work

supercapacitor with the samples used to obtain 115 and 171 F g^{-1}, respectively. The addition of the KOH activator concentration exhibits a significant increase in specific capacitance from 115 to 171 F g^{-1}. It also effectively forms and changes the pore structure of carbon monoliths with a higher concentration capable of increasing the specific surface area, as confirmed by N$_2$ gas adsorption/desorption analysis. KOH also allows the formation of macropores and mesopores, as confirmed by SEM analysis. The macropores have the ability to shorten the ion diffusion distance, while the mesopores provide fast ion electrolyte transport and large accessible surface areas for the formation of electrical double layers. This phenomenon causes a significant increase in specific capacitance from sample MG0.3 to MG0.5. This obtained

specific capacitance is relatively similar to other sources which are shown in table 3.

The energy and power density of the electrode super-capacitor were evaluated by standard equations (1) and (2) [51, 52] based on specific capacitance data, as shown in table 2.

$$E = \frac{C_{sp}V^2}{7.2},\qquad(1)$$

$$P = \frac{3600E}{\Delta t}.\qquad(2)$$

Where C_{sp} is the specific capacitance, V is the discharge voltage, and Δt is the discharge time (s).

Adv. Nat. Sci.: Nanosci. Nanotechnol. **12** (2021) 035013

R Taslim *et al*

The maximum energy and power density found in the MG0.5 sample were as high as 23.75 Wh kg^{-1} and 85.58 W kg^{-1}, respectively. The high energy and power density of the MG0.5 supercapacitor cell are mainly attributed to its high specific capacitance. Therefore, the symmetric supercapacitors based on porous carbon materials possess excellent electrochemical performances.

Figures 7(a) and (b) show the CV curves for samples MG0.3 and MG0.5 in the variation of scan rate ranging from 1 to 10 mV s^{-1}. All samples show rectangular shapes, which show that supercapacitor electrodes have the ability to transport ions relatively fast. A significant increase in the current density was also observed, which is attributed to the unique hierarchical pore structure and good conductivity of the supercapacitor electrodes. Figure 7(c) shows the specific capacitance versus the scan rate variations for all the samples. The increasing scan rates occurred due to the gradual decrease in specific capacitance because of the variety of controlling factors, which include the pore size distribution, a combination of micro- and mesopores, and specific surface areas. This is normally found in electrochemical double-layer capacitors.

4. Conclusion

In conclusion, this study analyses the cost-effectiveness associated with the one-stage integrated pyrolysis and KOH impregnation in the preparation of porous activated carbon derived from mission grass biomass waste. The porous carbon monolith comprises amorphous and interconnected macroporous and mesoporous structures. The study also shows that the addition of KOH concentration increased the specific surface area from 152.072 to 266.159 m^2 g^{-1} in the MG0.5 sample. Meanwhile, the symmetric capacitor double layers exhibit a rather high charge storage capacity with a specific capacitance of 171 F g^{-1} at a scan rate of 1 mV s^{-1} in a two-electrode system. Furthermore, the MG-0.5 sample shows high energy and power densities of 23.75 Wh kg^{-1} and 96.94 W kg^{-1}, respectively in a coin-type symmetric device. Therefore, the porous carbon derived from mission grass with effective-cost, sustainable, and abundant resource has potential for the supercapacitor energy storage application.

Acknowledgments

References

[1] Young C, Park T, Yi J W, Kim J, Hossain M S A, Kaneti Y V and Yamauchi Y 2018 *ChemSusChem* **11** 3546

[2] Zhang S *et al* 2020 *Chem. Eng. J.* **396** 125154

[3] Burke A 2000 *J. Power Sources* **91** 37

[4] González A, Goikolea E, Barrena J A and Mysyk R 2016 *Renew. Sustain. Energy Rev.* **58** 1189

[5] Miller E E, Hua Y and Tezel F H 2018 *J. Energy Storage* **20** 30

[6] Young C, Kim J, Kaneti Y V and Yamauchi Y 2018 *ACS Appl. Energy Mater.* **1** 2007

[7] Chen T, Li M, Zhou L, Ding X, Lin D, Duan T, Yang G, He R and Zhu W 2020 *ACS Sustain. Chem. Eng.* **8** 6458

[8] Poonam S K, Arora A and Tripathi S K 2019 *J. Energy Storage* **21** 801

[9] Tan H, Tang J, Kim J, Kaneti Y V, Kang Y M, Sugahara Y and Yamauchi Y 2019 *J. Mater. Chem. A* **7** 1380

[10] Iro Z S, Subramani C and Dash S S 2016 *Int. J. Electrochem. Sci.* **11** 10628

[11] Zhai Y, Dou Y, Zhao D, Fulvio P F, Mayes R T and Dai S 2011 *Adv. Mater.* **23** 4828

[12] Li X and Wei B 2013 *Nano Energy* **2** 159

[13] Gurmeet S and Amrita P 2015 *J. Pharmacogn. Phytochem. JPP* **5** 8

[14] Abioye A M and Ani F N 2015 *Renew. Sustain. Energy Rev.* **52** 1282

[15] González-García P 2018 *Renew. Sustain. Energy Rev.* **82** 1393

[16] Rangabhashiyam S and Balasubramanian P 2019 *Ind. Crops Prod.* **128** 405

[17] Li Y, Wang X and Cao M 2018 *J. CO$_2$ Util.* **27** 204

[18] Zhang W L, Xu J H, Hou D X, Yin J, Liu D B, He Y P and Lin H B 2018 *J. Colloid Interface Sci.* **530** 338

[19] Azwar E, Wan Mahari W A, Chuah J H, Vo D V N, Ma N L, Lam W H and Lam S S 2018 *Int. J. Hydrogen Energy* **43** 20811

[20] Apriwandi A, Agustino A, Taer E and Taslim R 2020 *J. Phys. Conf. Ser.* **1655** 16

[21] Taer E, Natalia K, Apriwandi A, Taslim R, Agustino A and Farma R 2020 *Adv. Nat. Sci. Nanosci. Nanotechnol.* **11** 025007

[22] Wang T *et al* 2020 *Cell Reports Phys. Sci.* **1** 100079

[23] Tatijarern P, Prasertwasu S, Komalwanich T, Chaisuwan T, Luengnaruemitchai A and Wongkasemjit S 2013 *Bioresour. Technol.* **143** 423

[24] Saka C 2012 *J. Anal. Appl. Pyrolysis* **95** 21

[25] Qu W, Xu Y, Lu A, Zhang X and Li W 2015 *Bioresour. Technol.* **189** 285

[26] Fan Y, Cai Y, Li X, Jiao L, Xia J and Deng X 2017 *Energy Convers. Manag.* **138** 106

[27] Gonzalez J, Roma S, Encinar J M and Martı G 2009 *J. Anal. Appl. Pyrolysis* **85** 134

[28] Uysal T, Duman G, Onal Y, Yasa I and Yanik J 2014 *J. Anal. Appl. Pyrolysis* **108** 47

[29] Yahya M A, Al-qodah Z and Ngah C W Z 2015 *Renew. Sustain. Energy Rev.* **46** 218

[30] Taer E, Taslim R, Mustika W S, Kurniasih B, Agustino and Afrianda A Apriwandi 2018 *Int. J. Electrochem. Sci.* **13** 8428

[31] Mohammed A A, Chen C and Zhu Z 2019 *J. Colloid Interface Sci.* **538** 308

[32] Boujibar O, Ghosh A, Achak O, Chafik T and Ghamouss F 2019 *J. Energy Storage* **26** 100958

[33] Jiang W, Pan J and Liu X 2019 *J. Power Sources* **409** 13

[34] Deng J, Xiong T, Wang H, Zheng A and Wang Y 2016 *ACS Sustain. Chem. Eng.* **4** 3750

[35] Cai Y, Luo Y, Dong H, Zhao X, Xiao Y, Liang Y, Hu H, Liu Y and Zheng M 2017 *J. Power Sources* **353** 260

[36] Yallappa S, Shivakumar M, Nagashree K L, Dharmaprakash M S, Vinu A and Hegde G 2018 *J. Electrochem. Soc.* **165** H614

[37] Liu Y, Wang Y, Zhang G, Liu W, Wang D and Dong Y 2016 *Mater. Lett.* **176** 60

[38] Xue M, Lu W, Chen C, Tan Y, Li B and Zhang C 2019 *Mater. Res. Bull.* **112** 269

[39] Sing K S W 1982 *Pure Appl. Chem.* **54** 2201

[40] Ahmed S, Ahmed A and Rafat M 2018 *J. Saudi Chem. Soc.* **22** 993

[41] Muniandy L, Adam F, Rahman A and Ng E 2014 *Microporous Mesoporous Mater.* **197** 316

[42] Zhang G, Chen Y, Chen Y and Guo H 2018 *Mater. Res. Bull.* **102** 391

[43] Ayinla R T, Dennis J O, Zaid H M, Sanusi Y K, Usman F and Adebayo L L 2019 *J. Clean. Prod.* **229** 1427

[44] Wang Y, Qu Q, Gao S, Tang G, Liu K, He S and Huang C 2019 *Carbon N. Y.* **155** 706

[45] Wei H *et al* 2020 *J. Alloys Compd.* **820** 153111

[46] Contescu C I, Adhikari S P, Gallego N C and Evans N D 2018 *J. Carbon Res.* **4** 9

[47] Kim C, Lee J, Kim J and Yang K 2006 *Korean J. Chem. Eng.* **23** 592

[48] Taer E, Apriwandi A, Ningsih Y S, Taslim R and Agustino A 2019 *Int. J. Electrochem. Sci.* **14** 2462

[49] Xiao C, Zhang W, Lin H, Tian Y, Li X, Tian Y and Lu H 2019 *New Carbon Mater.* **34** 341

[50] Scott K 2016 Electrochemical principles and characterization of bioelectrochemical systems *Microbial Electrochemical and Fuel Cells* (Newcastle upon Tyne: Elsevier) pp 29–66

[51] Sun Q, Jiang T, Zhao G and Shi J 2019 *Int. J. Electrochem. Sci.* **14** 1

[52] Men B, Guo P, Sun Y, Tang Y, Chen Y, Pan J and Wan P 2019 *J. Mater. Sci.* **54** 2446

[53] Subramanian V, Luo C, Stephan A M, Nahm K S, Thomas S and Wei B 2007 *J. Phys. Chem. C* **111** 7527

[54] Yang S, Wang S, Liu X and Li L 2019 *Carbon N. Y.* **147** 540

[55] Song G G, Yang J, Liu K X, Qin Z and Zheng X C 2021 *Diam. Relat. Mater.* **111** 108162

[56] Yang V, Senthil R A, Pan J, Khan A, Osman S, Wang L, Jiang W and Sun Y 2019 *J. Electroanal. Chem.* **855** 113616

[57] Kumar T R, Senthil R A, Pan Z, Pan J and Sun Y 2020 *J. Energy Storage* **32** 101903

[58] Duan B, Gao X, Yao X, Fang Y, Huang L, Zhou J and Zhang L 2016 *Nano Energy* **27** 482